Cell Reports
Physical Science

Report

Sodiation anodes derived from 2D transition-metal dichalcogenides

Graphical abstract

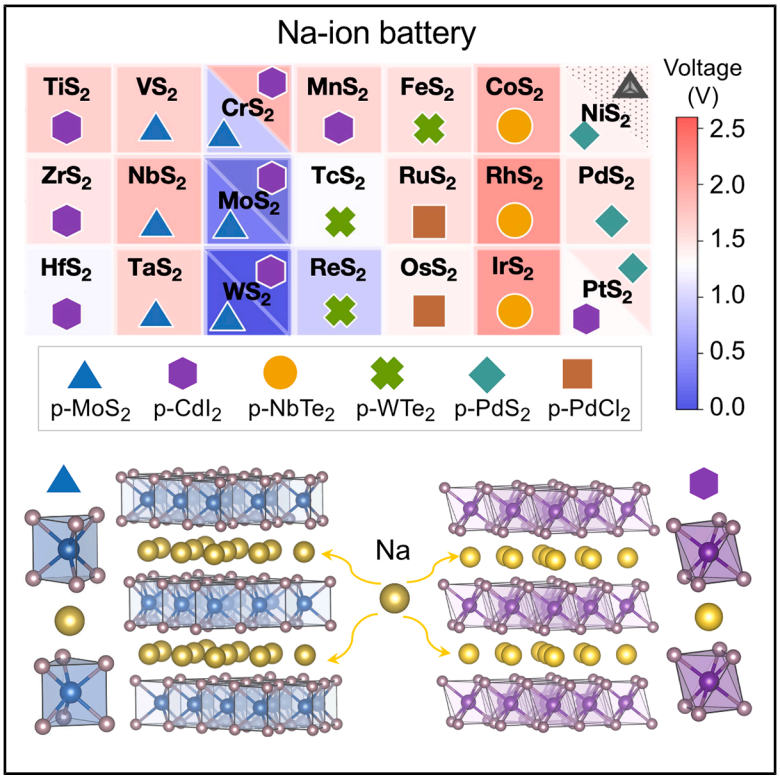

Highlights

- Voltage map of layered transition-metal dichalcogenides for Na-ion batteries
- Exhibiting competing phases upon sodiation, especially in groups VIB and VIIIB
- $MoSe_2$, WSe_2, $MoTe_2$, and WTe_2 show promise as phase-stable anodes

Authors

Jiangming Cao, Michael P. Mercer, Andrea Silva, Denis Kramer

Correspondence

d.kramer@hsu-hh.de

In brief

Next-generation sodium-ion batteries (SIBs) require improved anodes beyond hard carbon. Cao et al. report Na intercalation voltages for 63 layered transition-metal sulfides, selenides, and tellurides obtained from high-throughput density functional theory, clarifying the potential of this chemical space for scalable sodiation anodes.

Cao et al., 2026, Cell Reports Physical Science 7, 103252
May 20, 2026
https://doi.org/10.1016/j.xcrp.2026.103252

CellPress

Please cite this article in press as: Cao et al., Sodiation anodes derived from 2D transition-metal dichalcogenides, Cell Reports Physical Science (2026), https://doi.org/10.1016/j.xcrp.2026.103252

Cell Reports
Physical Science

CellPress
OPEN ACCESS

Report

Sodiation anodes derived from 2D transition-metal dichalcogenides

Jiangming Cao,[1] Michael P. Mercer,[2] Andrea Silva,[3,4] and Denis Kramer[1,5,*]
[1]Helmut-Schmidt-University Hamburg, University of the Armed Forces, Hamburg, Germany
[2]Lancaster University, Department of Chemistry, Lancaster, UK
[3]CNR-IOM, Trieste, Italy
[4]International School for Advanced Studies (SISSA), Trieste, Italy
[5]Lead contact
*Correspondence: d.kramer@hsu-hh.de
https://doi.org/10.1016/j.xcrp.2026.103252

SUMMARY

Sodium-ion batteries (SIBs) use more abundant materials than lithium-ion batteries, promising lower cost and better scalability. Challenges with hard carbon, however, motivate the development of alternative anodes. Layered transition-metal dichalcogenides (TMDs) show promise, but a conclusive consensus regarding TMDs has yet to emerge. Here, we report computed Na intercalation voltages of 63 layered TMDs. Group VIB TMDs show the lowest Na intercalation voltages, but competing phases potentially limit stability, which is closely linked to TM *d*-orbital occupation. More generally, low-voltage Na intercalation requires high-energy sodiated phases, which limits structural complexity, as complex chemical spaces provide more opportunity to lower crystal energies through phase changes. Less common systems, including $MoSe_2$, $MoTe_2$, and WSe_2, show attractive intercalation voltages with a lower likelihood of phase transitions. Hence, these systems might bear potential for application in SIBs, albeit with implied challenges regarding cost and abundance.

INTRODUCTION

Lithium-ion batteries (LIBs) have created a technological revolution by increasing the available energy density for portable devices and enabling automotive electrification. The cost of the raw materials involved in LIB manufacture—and the belief that lithium is relatively scarce—raises challenges for LIB applications in stationary storage and large-scale transport applications, such as in the maritime sector.[1–3] In sodium-ion batteries (SIBs), lithium is substituted with highly abundant sodium.[4] Like LIBs, SIBs consist of an organic electrolyte and various, often layered transition-metal oxides as the cathode material.[5,6] However, SIBs still have poor cycling stability and low capacity electrode materials. In this respect, it is indispensable to find appropriate electrode materials for advanced SIBs, including both cathode and anode materials. A particular challenge is finding appropriate anode materials for SIBs because the typical anode material for LIBs, graphite, does not intercalate a significant amount of sodium.[7] Hard carbons are currently considered the anode material with the most commercial promise.[8–15] However, the high surface area and inherent structural disorder of hard carbon are associated with severe degradation issues,[16,17] motivating the exploration of alternative anode materials.

Layered transition-metal dichalcogenides (TMDs) have evoked widespread attention as promising electrode materials,[18–20] particularly as potential anode materials. For example, the electrochemical performance of sodiating MoS_2, a widely investigated TMD, has been studied intensively using experiments and theory.[21–28] In general, the transition-metal M is coordinated with several chalcogen atoms (X = S, Se, and Te) in TMDs, allowing for various structures with composition MX_2, as is readily demonstrated by the polymorphism of MoS_2. A thorough investigation of this chemical space, therefore, has to take structural variability into account, even when experimental information is missing.

The crystal structures of a large range of 2D materials, derived from experimentally known 3D compounds, were investigated by Mounet et al. using high-throughput calculations based on van der Waals (vdW) density functional theory (DFT).[29] Building on that work, Silva et al. used DFT to compute Pettifor maps for metal sublattice alloys in several 2D TMD prototypes.[30,31] From this database of 2D-TMDs, layered TMDs can be constructed by simply stacking layers. Similarly, sodiated layered TMDs can be constructed by alternating TMD and Na layers. However, the sheer number of possible configurations necessitates a computational screening method as presented in this work, even when only considering the structures at zero and full sodiation.

The six prototypes reported by Silva et al.[30] to form 2D TMDs with different coordination environments are taken into consideration here, as shown in Figure 1A: p-MoS_2 (prismatic), p-CdI_2 (octahedral), p-$NbTe_2$ (parallel arranged octahedral), p-WTe_2 (in-plane distorted octahedral), p-PdS_2 (square planar), and p-$PdCl_2$ (octahedral with distorted axial and equatorial bonds).

Please cite this article in press as: Cao et al., Sodiation anodes derived from 2D transition-metal dichalcogenides, Cell Reports Physical Science (2026), https://doi.org/10.1016/j.xcrp.2026.103252

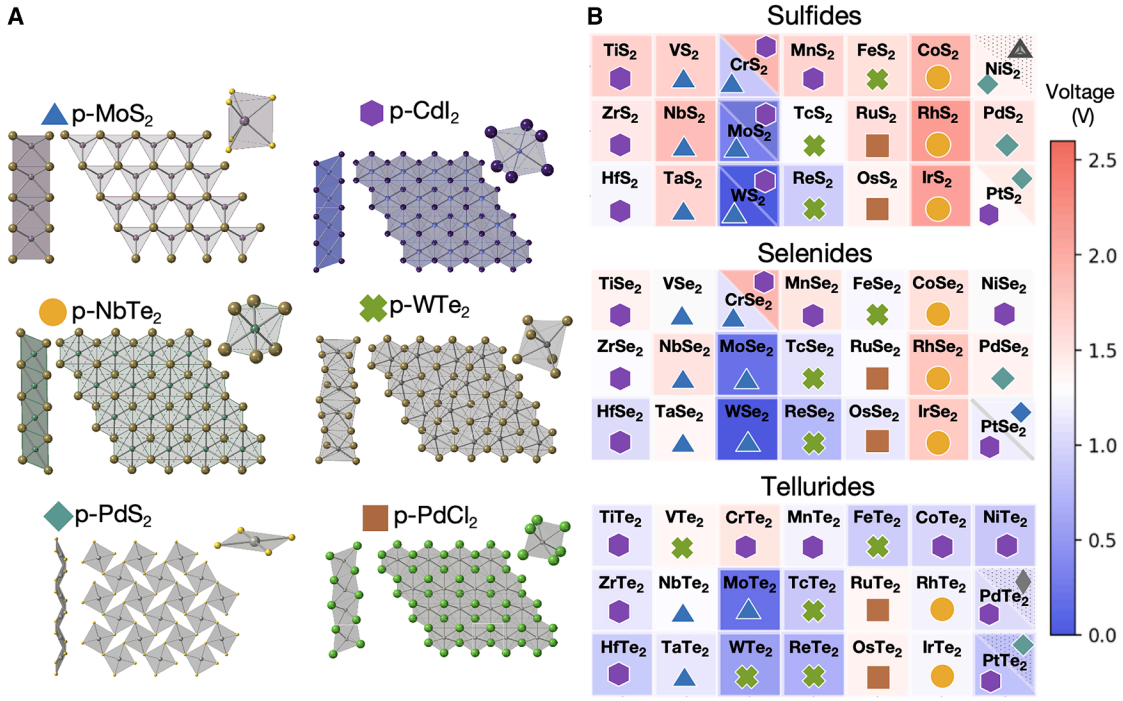

Figure 1. Periodic table of sodiation voltages of layered TMDs

(A) The six MX_2 prototypes and associated symbols: p-MoS_2, prismatic; p-CdI_2, octahedral; p-$NbTe_2$, parallel arranged octahedral coordination; p-WTe_2, in-plane distorted octahedral; p-PdS_2, square planar; p-$PdCl_2$, octahedral with distorted axial and equatorial bonds.

(B) The sodiation voltage of layered TMDs. The color bar on the right reports the voltage value vs. $Na|Na^+$ from blue to red. Chemistries with phase transition are identified by two voltage values and crystal structure symbols, respectively. The dotted regions in the top right of NiS_2, $PdTe_2$, and $PtTe_2$ denote compounds that spontaneously underwent phase transition during DFT structure optimization, cf. supplemental information for further details.

Among these, p-MoS_2 (2H phase) and p-CdI_2 (1T phase) are the most common structures.[32–35] Transition metals are coordinated with six chalcogen atoms in the p-MoS_2 prototype, forming triangular prisms, and MX_2 layers are stacked in AB order. Transition-metal atoms in p-CdI_2 adopt an octahedral coordination.

By computationally sodiating stable 2D-TMDs, Na intercalation voltages of the whole series of layered 3D-TMDs ($NaMX_2$) were calculated from first principles. The Na intercalation voltage serves as a guide for identifying anode materials for SIBs with high energy density and compatibility with the stability window of organic electrolytes. Finally, considering a range of host structures across chemistries enables the identification of systems that likely undergo phase transitions during sodiation, which is taken as a warning sign that durability during battery cycling might be limited. Taken together, this information provides an overview of likely electrochemical performance and structural properties of layered TMDs as SIB intercalation materials.

RESULTS AND DISCUSSION

Ground-state structures and sodiation potentials

The ground-state prototypes computed by DFT are shown in Figure 1A. Figure 1B shows a periodic table of Na intercalation voltages vs. metallic sodium for each compound (see methods and Equation 4 for details). The symbols indicate the stable prototypes for each compound, using the same convention as in Figure 1A. In a few cases, described further below, the intercalated compound was found to be stable in a different phase than the empty host, and therefore, a phase transition is expected (see also Figures S1 and S2 for the energetics of these transformations). For these cases, two voltage values are reported: the lower voltage assumes stability of the empty host after sodiation and the higher voltage takes the phase transition into account. The second symbol in the top right corner designates the stable sodiated phase. In both cases, the lowest energy phase MX_2 is used as a reference state in Equation 6 (further details are provided in the methods).

Layered TMDs intercalate Na over a broad range of voltages, ranging from close to zero to approximately +2.5 V vs. $Na|Na^+$. Two broad trends can be identified: (1) sulfides intercalate Na at higher voltages than the corresponding selenides and tellurides and (2) intercalation voltages tend to be lowest for group VIB TMs and increase toward the left and right in the periodic table.

TiS_2, for instance, intercalates Na at a higher voltage than $TiSe_2$, which in turn has a more positive intercalation voltage than $TiTe_2$. Similar observations can be made for almost all TMs that do not undergo phase transitions. A notable exception is tungsten, with WTe_2 intercalating Na at higher potentials than WSe_2, which can be attributed to tungsten selenide and telluride crystallizing in different crystal structures. Nonetheless, the

Please cite this article in press as: Cao et al., Sodiation anodes derived from 2D transition-metal dichalcogenides, Cell Reports Physical Science (2026), https://doi.org/10.1016/j.xcrp.2026.103252

voltages of sodiating WX_2 are below 1 V vs. $Na|Na^+$, making tungsten appear to be one of the two technologically most promising TMs. The other is molybdenum, as the MoX_2 compounds also tend to intercalate Na at voltages below 1 V vs. $Na|Na^+$. The early and late transition-metal sulfides generally do not provide intercalation voltages below 1 V. Some of them could even be considered low-voltage cathode chemistries. This dependence of intercalation voltage on TM group is less pronounced in the selenides and tellurides. In particular, the tellurides show relatively low intercalation voltages across the entire *d*-block.

Focusing on group VIB again, the intercalation voltages for CrS_2, MoS_2, WS_2, and $CrSe_2$ in the p-MoS_2 prototype are 0.90, 0.32, 0.01, and 1.09 V, respectively, as indicated in the bottom left corner of each compound in Figure 1B. They all appear to be viable anode chemistries at first sight. However, the lowest energy phase for the intercalated compounds, $NaMX_2$, differs from that of the empty host, MX_2, indicating that these compounds are liable to undergo a phase transition during intercalation with potential implications for the sodiation potential. The voltages after accounting for the phase change are 1.90, 0.34, 0.01, and 1.90 V, respectively, as indicated in the top right corner of each compound. All these compounds favor octahedral coordination within the p-CdI_2 prototype after sodiation, even though the most stable phase of the empty host is p-MoS_2 in all cases. Indeed, the energetic advantage of p-CdI_2 over p-MoS_2 in the sodiated phases is so significant that, for CrS_2 and $CrSe_2$, voltages increase to values that render these compounds unsuitable as anode materials for SIBs. These competing phases also raise questions about the stability and viability of these materials during cycling, even when the voltage increase is negligible, as is the case for MoS_2 and WS_2.

The remaining compounds in group VIB, namely $MoSe_2$, WSe_2, $MoTe_2$, and WTe_2, are not predicted to undergo phase transitions and remain in the same structure without and with sodium (as shown in Figure S2). The absence of a phase transition is a potentially useful feature for long cycle life in energy storage applications, in combination with the low intercalation voltages of $MoSe_2$, WSe_2, $MoTe_2$, and WTe_2 (0.22, 0.01, 0.19, and 0.55 V, respectively) for battery applications.

Another interesting case is TiS_2, which is in group IVB. This compound remains in an octahedral configuration, but the MX_2 layers undergo a shift from AA stacking to AB stacking upon sodiation. This transformation happened spontaneously during structure optimization, with the structures shown in Figure S3. This phase transition is known from experiments,[36–39] as discussed further below. A few other structures with similar stacking transitions were found, and these are summarized in the supplemental information.

Group VIIIB (rightmost column) is another group that shows a high propensity for phase transitions. NiS_2 crystallizes in the square-planar configuration (p-PdS_2 prototype), while the sodiated $NaNiS_2$ shows distorted tetrahedral coordination. The coordination of $PdTe_2$ changes from octahedral (p-CdI_2 prototype) to distorted octahedral with an elongated vertical axis. The ground-state structures of PtX_2 (PtS_2, $PtSe_2$, and $PtTe_2$) are octahedral (p-CdI_2 prototype), but the most stable sodiated compound $NaPtX_2$ is square planar (p-PdS_2 prototype). The respective structures are provided in Figure S4.

Model Hamiltonian

To discuss and understand broad trends in chemical space, it is useful to recall a few notions of crystal field theory as a simplified energy model.

Crystal field theory is a semi-quantitative framework to rationalize the electronic structure of transition-metal complexes and, to a lesser degree, transition-metal compounds.[40,41] The 5-fold energetic degeneracy of the *d*-orbitals is lifted by next-neighbor ligands that shift the energies of individual *d*-orbitals according to geometric proximity. The interaction between *d*-orbitals and ligands is assumed to be purely electrostatic, though, making the theory most appropriate for highly localized electronic structures. The resultant split in energy levels is denoted by Δ. Orbital energies are shifted negative and positive relative to the barycenter of the *d*-manifold (i.e., the zero point of the energy scale). Orbital energies are expressed as a fraction of Δ, with the number and degeneracy of levels given by the local symmetry of the ligand field. Further, the electron-pairing energy, *P*, needs to be taken into account when electrons are paired in the same orbital. The energy is expressed as

$$E = \sum_i f_i \cdot \xi_i \cdot \Delta + n \cdot P, \qquad \text{(Equation 1)}$$

where n is the number of electron pairs and f_i and ξ_i are the occupancy and relative position of the energy levels, respectively. Summation is over all energy levels. The relative energies of the *d*-orbitals for ligands in prismatic, octahedral, square-planar, and tetrahedral coordination are covered in detail in the literature.[32,40–45] Usual values of Δ are in the range of 1 … 4 eV for transition-metal complexes. There is generally less data available for electron-pairing energies *P*, but they are accepted to be smaller than Δ by a factor of four to maybe ten. Besides providing a convenient framework to rationalize the relative stability of local TM coordination, even subtle effects such as Jahn-Teller distortions[46,47] can be rationalized with crystal field theory. Nonetheless, it has to be emphasized that the framework has limited utility for strongly covalent compounds and, hence, is used here mostly to discuss trends.

Prismatic-to-octahedral phase transition in group VIB

The energies of the sodiated and unsodiated phases of $CrSe_2$ in the p-MoS_2 (prismatic, 2H) and p-CdI_2 (octahedral, 1T) prototypes are shown in Figure 2A. Similar to CrS_2, MoS_2, and WS_2 (Figure S4A), the intercalated compound is stable in octahedral coordination, while the empty host is prismatic. All these compounds undergo a transition from 2H to 1T, resulting in an increase in voltage. This result is in good agreement with previously reported results for MoS_2.[23,24] The energy above the hull for the selected Na-M-X system can be found in Table S6, confirming the stability of these materials against decomposition into other non-layered phases. The Na-Cr-Se phase diagram is plotted in Figure S12 as an example, according to the energy above the hull in Table S6 and Bartel.[48]

The *d*-orbital splitting according to crystal field theory for these compounds—with the exception of CrS_2, whose magnetic moment indicates a different ordering of the crystal field stabilization energy (CFSE) levels (cf. Table S5 and Figure S6)

Please cite this article in press as: Cao et al., Sodiation anodes derived from 2D transition-metal dichalcogenides, Cell Reports Physical Science (2026), https://doi.org/10.1016/j.xcrp.2026.103252

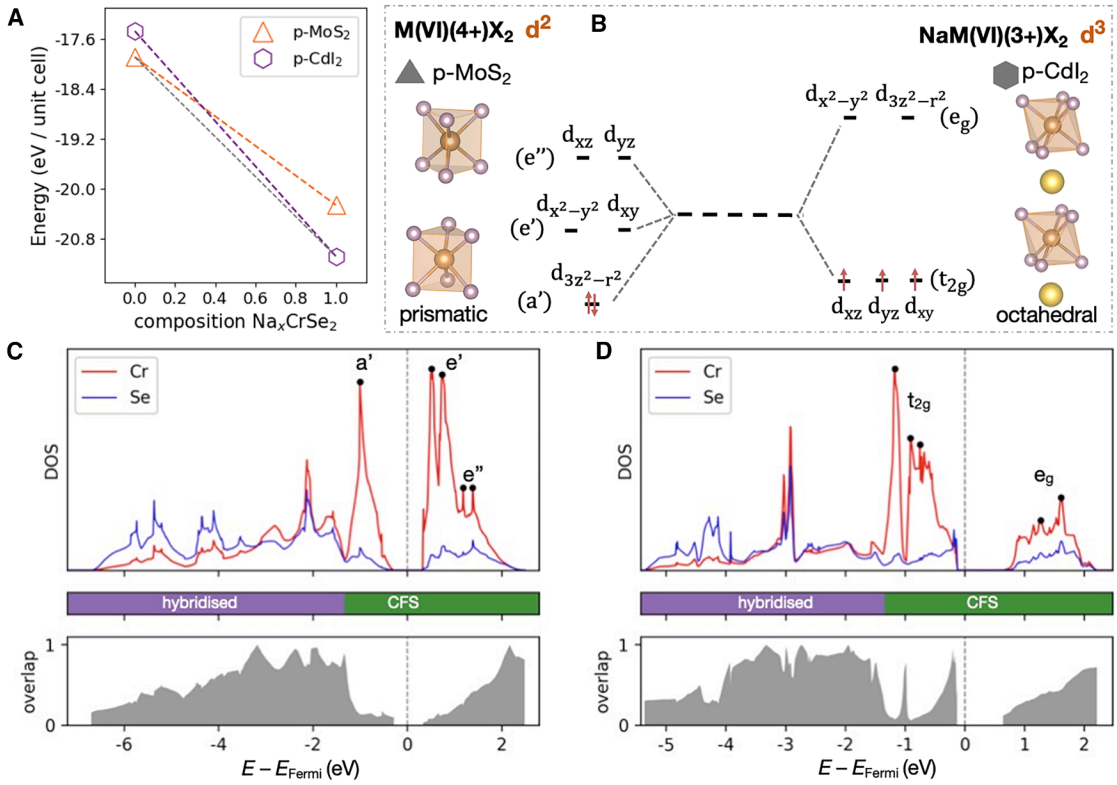

Figure 2. Energetics and electronic structure of Na_xCrSe_2

(A) Energy diagram, (B) crystal field splitting (CFS) of the *d*-orbitals in prismatic and octahedral coordination, (C) density of states in prismatic $CrSe_2$, and (D) density of states in octahedral $NaCrSe_2$. The top images in (C) and (D) report the DOS projected on the *d*-manifold of Cr (red curve) and the p-manifold of Se (blue line). The dashed gray lines indicate the Fermi level. The black dots mark the peaks attributed to CFS levels in (B). The middle images highlight the energy windows identified as hybridization-like and CFS-like. The bottom images show the overlap between the DOS projected on Cr and Se atoms, as defined in Figure S6.

due to a slightly different geometry of the prismatic environment[45]—is depicted in Figure 2B for the unsodiated structure (p-MoS_2 prototype) and the sodiated structure after phase transition (p-CdI_2 prototype). The unsodiated compounds have a formal valence of M^{4+} and a d^2 electron configuration. Both electrons occupy the a' level (i.e., the $d_{3z^2-r^2}$ orbital) because it is located between the ligands (X = S, Se, and Te) in p-MoS_2. So the repulsive force between the *d*-electrons and the ligands is low.

Upon sodium intercalation, the transition metal reduces from M^{4+} to M^{3+} (d^3). The extra electron has to occupy the e' level, located in the plane between the ligands, in the prismatic environment (see Figure 2B, left). This results in an energy gain of

$$2\cdot(-0.534\,\Delta_o) + P + 1\cdot(-0.089\,\Delta_o) = -11.57\,Dq + P \quad \text{(Equation 2)}$$

or $2{\cdot}E_{a'} + P + 1{\cdot}E_{e'} = -11.57\,Dq + P$, where $\Delta_o = 10\,Dq$ is the splitting constant in octahedral coordination, which is related to the charge on the metal ion, the radial distribution of valence *d*-electrons, and the metal-ligand distance.[41]

The energy can be lowered in an octahedral environment, as depicted on the right-hand side of Figure 2B. The three electrons occupy the low-energy t_{2g} orbitals, avoiding the pairing penalty and yielding an energy gain of

$$3\cdot(-0.4\Delta_o) = -12\,Dq. \quad \text{(Equation 3)}$$

This is always lower than in prismatic coordination because the pairing energy *P* is positive.

The CFS-based argument can be made quantitative by parameterizing the model Hamiltonian in Equation 1 from DFT calculations. The energy splitting between CFS levels can be obtained from the projected density of states (DOS) of $CrSe_2$ and $NaCrSe_2$ (see black circles in Figures 2C and 2D). The pairing energy *P* can be estimated by magnetization-constrained calculations (see Figure S7 for details). The energy levels with respect to the energy barycenter are $E_{a'} = -1.57$ eV, $E_{e'} = -0.05$ eV, and $P = 1.09$ eV in the prismatic environment and $E_{t_{2g}} = -0.95$ eV and $E_{e_g} = 1.38$ eV, respectively, in the octahedral environment. Hence, the model Hamiltonian yields the following energies (in eV): $E(CrSe_2\text{-prism}) = -2.05$, $E(CrSe_2\text{-oct}) = -1.91$, $E(NaCrSe_2\text{-prism}) = -2.10$, and $E(NaCrSe_2\text{-oct}) = -2.859$, which agrees with the ordering predicted qualitatively above.

Finally, some compounds in the nickel group show a similar tendency for phase transitions from octahedral to

square-planar configuration. As these compounds are less relevant to battery applications, this is discussed in terms of crystal field theory in the supplemental information for completeness.

Intercalation voltages of prismatic compounds in groups VB and VIB

Unsodiated hosts from groups VB and VIB tend to favor prismatic coordination. At the same time, they also tend to cluster at the opposite ends of the voltage scale. While prismatic group VIB compounds provide an opportunity to intercalate at voltages below 0.5 V vs. Na|Na^+, group VB compounds exhibit at least 1.0 V higher voltages despite the similar crystal structures and proximity in the periodic table.

This can also be rationalized using crystal field theory. Upon sodiating a d^1 compound from group VB, the additional electron occupies the remaining lowest a' energy level, and the energy difference due to d-orbital occupation is $-0.534\Delta_o + P$. As already explained, reduction of a d^2 transition metal from group VIB requires occupation of an e' energy level with an energy difference of $-0.089\ \Delta_o$. The spin pairing energy P raises the energy significantly less than the occupation of the higher energy e' level. In consequence, prismatic group VB compounds are more strongly stabilized by d-orbital occupation upon sodiation than group VIB compounds. This not only explains the absence of phase transitions in group VB but also explains the significantly higher voltages. Because formation energy and voltage are inversely related (see methods below), a lower-energy sodiated structure translates into a higher intercalation voltage, as nicely demonstrated by comparing group VB and group VIB voltages.

This highlights an important challenge when searching for low-voltage intercalation anodes in general. Low-voltage anode chemistries require high-energy sodiated phases. The more complex a chemical space is, the more possibilities likely exist for nature to find ways to lower the energy of the sodiated phase by adopting a different coordination or electronic configuration. Hence, the search should favor "simple" crystal structures or at least aim for kinetic stability (e.g., through strong covalent/ionic bonds).

Further trends in intercalation voltages

Group IVB compounds exhibit high intercalation voltages. Following the same reasoning as above, this can be rationalized with the d^1 configuration of the sodiated phase. Because the d^0 configuration of the unsodiated phase always implies single occupation of the lowest energy level after sodiation, these early transition-metal compounds cannot realize "unfavorable" electron configurations that lead to high energy structures and thus low voltages.

It is attractive to favor host compounds with fully occupied lowest energy levels in the crystal field theory picture to search for low-voltage anodes, because it implies energetically costly occupation of energy levels in the next highest d-band manifold (e.g., e_g instead of t_{2g} in octahedral environments) upon sodiation. The group of prismatic d^2 compounds already discussed is a case in point. However, the layered TMDs provide few other compounds where this is the case. There are no tetrahedral compounds for which one would look at low-spin d^4 compounds in group VIIIB. Alternatively, d^6 compounds in a low-spin octahedral configuration would qualify. Ni is the only group VIIIB element that favors octahedral coordination as selenide and telluride in the unsodiated as well as sodiated phases. However, the sodiated phases show fully spin-paired ground states (cf. Figure S5), which is irreconcilable with a d^7 configuration in the ionic picture underpinning crystal field theory. Hence, the expected strong covalent character of these compounds clearly invalidates the simple reasoning based on crystal field theory, in notable parallel to $LiNiO_2$.[49] Nonetheless, at least $NiTe_2$ is predicted to show a somewhat attractive intercalation voltage.

Finally, square-planar NiS_2 seems like a promising candidate. The splitting constant in the square-planar configuration is particularly large, and the two lowest energy levels are fully occupied in a low-spin d^6 configuration. But like the prismatic group VIB compounds, the system suffers from a phase transition to a highly distorted structure in the sodiated phase.

High-spin configurations are less common. However, in octahedral coordination, d^3 compounds that favor high-spin configurations in d^4 configurations would be candidates. Manganese seems to be the only transition metal that favors high-spin states in d^3 as well as d^4 configurations in every MnX_2 chalcogenide in the octahedral p-CdI_2 prototype. But Mn-based chemistries are predicted by DFT to show relatively high voltages. Mn is known to be strongly Jahn-Teller active, and the relatively high voltages of MnX_2 compounds likely result from strong structural relaxations.

Experimental results for sodiation of TMDs in group VIB

The simulation results above suggest, at first glance, that group VIB compounds are the most promising candidates for Na-ion intercalation anodes of all the TMDs, as these have the lowest Na intercalation voltages.

The MoS_2 system, in particular, has been thoroughly examined experimentally.[23–25] The presence of competing phases leading to the 2H → 1T transformation upon sodiation is experimentally confirmed.[23–25] Additionally, while not examined in the present work, the resulting phase boundaries impede the dynamics of sodiation[23] and result in structural changes after the first sodiation cycle.[24,25] In combination, these factors raise serious questions about the viability of MoS_2 (in addition to CrS_2,[50] WS_2,[51] and $CrSe_2$) as Na-ion intercalation anode materials.

The computed voltage values for WS_2 are similar to those of MoS_2, as is the predicted phase transformation. This chemistry has previously been studied both experimentally and theoretically.[51] Results are in good agreement with our predictions. WS_2 nano-flakes crystalize with W in prismatic coordination, but W adopts octahedral coordination in $NaWS_2$. Experimentally observed intercalation voltages are around 1.5 V vs. Na|Na^+, which is slightly above—but still in good agreement with—theoretical values.

The contrast between the calculated Na intercalation voltages of MoS_2 and CrS_2 is pronounced in Figure 1. The voltage of sodiating CrS_2 accounting for the 2H → 1T phase transition is 1.90 V. In fact, this voltage is among the highest of all TMDs reported in Figure 1B, indicating a strong stabilization of Cr in octahedral

configuration. Consequently, there has been some interest in using $NaCrS_2$ as a Na intercalation cathode material in its most stable 1T phase,[50] with the 1T → 2H transformation avoided by deintercalating only to $Na_{0.5}CrS_2$. $CrSe_2$ is predicted to behave very similarly to CrS_2. The electrochemical Na performance would therefore likely be similar, but experimental studies for comparison appear unavailable. Finally, the capacity-limiting phase transition could probably be avoided with $CrTe_2$ as cathode chemistry but likely at the cost of a lower voltage.

Predicted voltages in Figure 1 suggest some promise for $MoSe_2$, WSe_2, and $MoTe_2$ as anode materials, which have been explored experimentally far less than MoS_2. Additionally, the larger interlayer spacing in these materials compared with MoS_2 might result in improved intercalation dynamics. Morales et al. examined Na-ion intercalation in $MoSe_2$, finding a 2H → 1T transformation during sodiation via *operando* X-ray diffraction (XRD),[52] with more recent experimental work also reporting the same transformation.[53] Interestingly, this phase transition is not predicted in Figure 1. The p-MoS_2 structure (2H, prismatic) is calculated to be about 200 meV per formula unit (f.u.) lower in energy than the p-CdI_2 (1T, octahedral) structure (cf. supplemental information). This energy difference is larger than the usual uncertainty associated with DFT total energy calculations, suggesting that factors not included here, such as vibrational energy contributions, defects, or the presence of secondary phases such as carbon, might be relevant. However, it can also be noted that Morales et al. concluded the 2H → 1T phase transition based on an analogy to MoS_2 from a shift of the (002) reflection in XRD spectra, which is mostly governed by TM layer spacing rather than TM coordination in layered compounds. There is a substantial recent effort to crystallize the 1T phase through advanced synthesis routes,[54–56] but we were unable to find compelling direct evidence for an *in situ* transition between the two crystal structures during sodiation. In most cases, formation of a disordered or amorphous phase is reported upon sodiation. In terms of kinetics, 2H-$MoSe_2$ shows a higher Na interlayer barrier (approximately 1.4 eV) compared with Na diffusion along the $MoSe_2$ surface, suggesting challenges of slow diffusion between layers that might impede practical implementation of $MoSe_2$ as a Na-ion intercalation electrode.[57]

Finally, although the lowest overall Na intercalation voltage is predicted for WSe_2 in Figure 1, there is only a limited number of experimental references available,[58,59] with no comparable *operando* studies to assess stability during operation, making it difficult to draw conclusions about thermodynamic stability, kinetic trends, or interphase stability for this system. Of course, practical concerns about the weight, abundance, and toxicity might make this compound—and selenides and tellurides in general—less attractive, as remarked in Tables S8–S10. Low diffusion barriers for Na on WSe_2 monolayers, on the order of 0.06 eV,[60,61] have been reported, suggesting that low-dimensional forms of this material might have potential for high-rate applications. However, the significantly higher interlayer diffusion barrier on the order of 0.6 eV again raises questions about the practical rate performance of these materials.[61] Comparable values of Na interlayer diffusion coefficients on the order of 0.3–0.4 eV were determined elsewhere across the MoX_2/WX_2 systems.[35]

Experimental results for sodiation of TMDs outside of group VIB

Few TMD candidates outside of group VIB are predicted to show Na intercalation voltages low enough to make them attractive as anode materials. Nevertheless, many of these candidates have been investigated experimentally, particularly the sulfides in period 4. These represent the lightest and also most Earth-abundant materials among the TMDs, in line with efforts to optimize gravimetric capacity.

TiS_2 has been extensively investigated as a Na-ion electrode material,[36,62,63] showing Na intercalation voltages on the order of 1.67 V as computed in this work. It is of interest because of its high conductivity,[38] large interlayer spacing,[37,62] and pronounced phase transformations due to layer shifts and distortions of the octahedral environment.[36–38] For these reasons, it remains an important material in the field for method development, but its intermediate sodium intercalation voltage limits its viability as either a positive or negative electrode material.

The same concerns apply to the rest of the period 4 transition-metal sulfides (with the possible exception of CrS_2, as mentioned above). VS_2,[64] MnS_2,[65] and FeS_2[66,67] showed very similar computed voltages on the order of 1.6 V in the present work, in good agreement with the cited experimental studies. Additionally, *operando* diffraction studies suggest solid-solution Na intercalation into Na_xVS_2 and Na_xFeS_2 ($0 \leq x \leq 1$) rather than additional phase transformations.[64,66] NbS_2, located in the same group and with the same crystal structure as VS_2, likewise remains in a stable phase during sodiation.[68] These findings are in good agreement with the results reported here.

Considerations of toxicity and abundance

Apart from pure performance considerations, Tables S8 and S10 summarize the abundance and toxicity of TMDs and reveal clear trends across the chalcogen series.[69,70] Sulfides are more abundant and better characterized than selenides, which are in turn more common than tellurides. This trend reflects both the higher natural abundance of sulfur relative to selenium and tellurium and the greater ease of synthesizing stable sulfide phases.

MoS_2, WS_2, TiS_2, NbS_2, and TaS_2 are widely abundant, experimentally verified, well established in the literature, and frequently studied due to their thermodynamic stability and straightforward synthesis.[69,71,72] Therefore, they have been extensively explored experimentally, allowing the development of detailed phase diagrams and structure-property relationships.

Sulfides and selenides of Zr, Hf, Cr, Fe, Ru, Co, and Ni are accessible but have been less systematically investigated.[69,70,72] Most studies report only synthesis and basic characterization, but the systematic understanding of their electrochemical and electronic properties remains limited. This intermediate abundance suggests they are promising candidates for further study, particularly in applications where common TMDs are insufficient.

Sparse or mostly predicted systems such as Tc, Re, Os, Ir, and Rh compounds are supported mainly by theoretical predictions

Please cite this article in press as: Cao et al., Sodiation anodes derived from 2D transition-metal dichalcogenides, Cell Reports Physical Science (2026), https://doi.org/10.1016/j.xcrp.2026.103252

and high-throughput calculations, with few experimental reports.[70,71] Their limited availability and possibly marginal thermodynamic stability hinder detailed study and necessitate continued computational screening and targeted experimental validation to assess their viability.

Promising chemistries beyond MoS_2

Finding a suitable Na-ion intercalation anode material to supersede hard carbon is highly challenging. Low-voltage intercalation chemistries require high-energy sodiated phases, which means unfavorable *d*-electron configurations for TMDs. This increases the likelihood of more stable competing phases upon sodiation, which will result in an increase in cell voltage, as is the case for many of the group VIB TMDs, including MoS_2. Additionally, those competing phases may lead to further detrimental behavior during cycling.

Even so, group VIB compounds seem most viable from an intercalation voltage point of view: the $MoSe_2$, WSe_2, $MoTe_2$, and WTe_2 systems appear to be promising anode materials because of their relatively low Na intercalation voltages (and apparent absence of phase changes). Of course, considerations of weight, abundance, and toxicity make these materials less viable. Thus, this part of the parameter space has been much less explored experimentally than the lighter and more abundant TMDs. Nonetheless, these should be examined in more detail because understanding of the stable phases across the periodic table and their effect on the Na intercalation voltage is likely to lead to alternative strategies to optimize TMD-based anodes, such as heterostructures and/or alloying.

Limitations of the study

This study is based on total energy DFT calculations with a limited search for competing phases and may not have considered all possible phases. Further, partial sodiation and sodiation potentials as functions of state of charge have not been considered. Predictions were solely validated against accessible experimental literature. This study did not comprise any experiments.

METHODS

Computational protocol

Layered TMDs were created and sodiated from a database of 2D prototypes originally derived and structurally optimized by DFT by Silva et al.,[30,31] which in turn was based on data from Mounet et al.[29] Layered, sodiated structures were derived using these layered hosts by introducing sodium via a procedure described in the supplemental information, illustrated in Figure S8. Properties of all TMDs were computed by DFT. All calculations were performed using the Perdew-Burke-Ernzerhof (PBE)[73] functional and projector augmented waves (PAWs)[74] to account for core electrons, as implemented in the Vienna *Ab initio* Simulation Package (VASP),[75–77] which is consistent with our earlier works.[30,31] Wave functions were expanded in a plane wave basis set with a cutoff energy of 650 eV. The Kohn-Sham equations were solved self-consistently with an energy convergence threshold of 10^{-6} eV. Structures were fully optimized until atomic forces were less than 10^{-2} eV/Å. During structure relaxation, the DFT-D2 correction scheme[78] was employed to account for interlayer vdW interactions and to ensure reasonable layer spacings.[25,79] However, for some of the structures, particularly the tellurides, the energy contribution from D2 was a substantial fraction of the total energy, raising concerns regarding the predictive power of total energy calculations employing this convenient but simplistic dispersion model. Therefore, relaxation and voltages are based on total energies without vdW correction. Overall, this resulted in some slight systematic shift of the voltage values, but the overall trends were not affected, as shown in Figure S11A and Tables S1 and S2. The effect of different vdW corrections is further described in more detail in the supplemental information (Figures S9–S11, Table S3, and the surrounding discussion).

In the interest of tractably establishing trends across the entire series of TMDs, we opted to use the commonly used PBE functional in this work. As an outlook, we suggest that future benchmarking studies using more sophisticated vdW-inclusive functionals would be valuable for refining energy-based predictions.

Computation of intercalation voltage

The intercalation voltage was computed as follows:

$$V = -\frac{\Delta H}{e}. \qquad \text{(Equation 4)}$$

The reaction enthalpy ΔH for the intercalation of TMDs with sodium, i.e.,

$$\mathrm{Na(s)} + \mathrm{MX_2(s)} \rightarrow \mathrm{NaMX_2(s)}, \qquad \text{(Equation 5)}$$

is determined by[80]

$$\Delta H = E(\mathrm{NaMX_2}) - (E(\mathrm{Na}) + E(\mathrm{MX_2})), \qquad \text{(Equation 6)}$$

where $E(\mathrm{NaMX_2})$ and $E(\mathrm{Na})$ are the total energies of sodiated bulk TMD and Na (body-centered cubic, bcc), respectively. Using the enthalpy H rather than the Gibbs free energy G as the thermodynamic potential is an approximation that neglects entropic contributions. However, as Equation 4 represents a phase equilibrium of solid phases without configurational degrees of freedom, differences in entropy are small and dominated by vibrational properties.

In some cases, described in the text above, a ground-state structure of the sodiated phase $NaMX_2$ with a space group distinct from the ground-state structure of the unsodiated phase MX_2 is reported. While ground-state structures of host layers were exhaustively determined by Silva et al.,[30,31] a limited investigation of phase stability was conducted here for sodiated phases based on available experimental data and chemical intuition, complemented by a harsh relaxation procedure: sodiated structures were initialized with a rather small layer spacing, which produced large initial forces acting on atoms after sodiation. These large initial forces were meant to allow the relaxation procedure to escape local energy minima and led to large initial volume expansions. Where structures did not return to the initial host structure upon convergence of the relaxation procedure, a more detailed investigation of phase stability was conducted.

RESOURCE AVAILABILITY

Lead contact

Requests for further information and resources should be directed to and will be fulfilled by the lead contact, Denis Kramer (d.kramer@hsu-hh.de).

Materials availability

This study did not generate any new materials.

Data and code availability

- DFT data have been deposited at Nomad and are publicly available as of the date of publication at Nomad: https://doi.org/10.17172/NOMAD/2026.01.26-1.
- The code for generating sodiated structures can be found in Data S1 as an archived file.
- Any additional information required to reanalyze the data reported in this paper is available from the lead contact upon request.

ACKNOWLEDGMENTS

We acknowledge funding through the DTEC.Bw project "Digital Materials Foundry." DFT calculations were performed on HSUper provided by the HPC.Bw project, likewise funded by DTEC.Bw — Digitalization and Technology Research Center of the Bundeswehr. DTEC.Bw is funded by the European Union – NextGenerationEU.

AUTHOR CONTRIBUTIONS

J.C. and A.S. performed the simulations. J.C. wrote the manuscript with D.K., M.P.M., and A.S. All authors discussed and analyzed the results. D.K. supervised the work.

DECLARATION OF INTERESTS

The authors declare no competing interests.

SUPPLEMENTAL INFORMATION

Supplemental information can be found online at https://doi.org/10.1016/j.xcrp.2026.103252.

Received: July 1, 2025
Revised: November 7, 2025
Accepted: March 18, 2026

REFERENCES

1. Tarascon, J.M., and Armand, M. (2001). Issues and challenges facing rechargeable lithium batteries. Nature *414*, 359–367. https://doi.org/10.1038/35104644.
2. Hesse, H., Schimpe, M., Kucevic, D., and Jossen, A. (2017). Lithium-ion battery storage for the grid—a review of stationary battery storage system design tailored for applications in modern power grids. Energies *10*, 2107.
3. Vandepaer, L., Cloutier, J., and Amor, B. (2017). Environmental impacts of lithium metal polymer and lithium-ion stationary batteries. Renew. Sustain. Energy Rev. *78*, 46–60.
4. Kundu, D., Talaie, E., Duffort, V., and Nazar, L.F. (2015). The emerging chemistry of sodium ion batteries for electrochemical energy storage. Angew. Chem. Int. Ed. Engl. *54*, 3431–3448. https://doi.org/10.1002/anie.201410376.
5. Tapia-Ruiz, N., Armstrong, A.R., Alptekin, H., Amores, M.A., Au, H., Barker, J., Boston, R., Brant, W.R., Brittain, J.M., Chen, Y., et al. (2021). 2021 roadmap for sodium-ion batteries. JPhys Energy *3*, 031503. https://doi.org/10.1088/2515-7655/ac01ef.
6. Xie, F., Xu, Z., Guo, Z., and Titirici, M.M. (2020). Hard carbons for sodium-ion batteries and beyond. Prog. Energy *2*, 042002. https://doi.org/10.1088/2516-1083/aba5f5.
7. Metrot, A., Guerard, D., Billaud, D., and Herold, A. (1980). New results about the sodium-graphite system. Synth. Met. *1*, 363–369. https://doi.org/10.1016/0379-6779(80)90071-5.
8. Stratford, J.M., Kleppe, A.K., Keeble, D.S., Chater, P.A., Meysami, S.S., Wright, C.J., Barker, J., Titirici, M.M., Allan, P.K., and Grey, C.P. (2021). Correlating local structure and sodium storage in hard carbon anodes: Insights from pair distribution function analysis and solid-state nmr. J. Am. Chem. Soc. *143*, 14274–14286.
9. Sun, N., Guan, Z., Liu, Y., Cao, Y., Zhu, Q., Liu, H., Wang, Z., Zhang, P., and Xu, B. (2019). Extended adsorption–insertion model: A new insight into the sodium storage mechanism of hard carbons. Adv. Energy Mater. *9*, 1901351.
10. Sun, N., Qiu, J., and Xu, B. (2022). Understanding of sodium storage mechanism in hard carbons: Ongoing development under debate. Adv. Energy Mater. *12*, 2200715.
11. Zhao, R., Sun, N., and Xu, B. (2021). Recent advances in heterostructured carbon materials as anodes for sodium-ion batteries. Small Struct. *2*, 2100132.
12. Stevens, D.A., and Dahn, J.R. (2000). High capacity anode materials for rechargeable sodium-ion batteries. J. Electrochem. Soc. *147*, 1271. https://doi.org/10.1149/1.1393348.
13. Stevens, D.A., and Dahn, J.R. (2001). The mechanisms of lithium and sodium insertion in carbon materials. J. Electrochem. Soc. *148*, A803. https://doi.org/10.1149/1.1379565.
14. Mercer, M.P., Affleck, S., Gavilán-Arriazu, E.M., Zülke, A.A., Maughan, P.A., Trivedi, S., Fichtner, M., Reddy Munnangi, A., Leiva, E.P.M., and Hoster, H.E. (2022). Sodiation of hard carbon: How separating enthalpy and entropy contributions can find transitions hidden in the voltage profile. ChemPhysChem *23*, e202100748.
15. Mercer, M.P., Nagarathinam, M., Gavilán-Arriazu, E.M., Binjrajka, A., Panda, S., Au, H., Crespo-Ribadeneyra, M., Titirici, M.M., Leiva, E.P.M., and Hoster, H.E. (2023). Sodiation energetics in pore size controlled hard carbons determined via entropy profiling. J. Mater. Chem. A *11*, 6543–6555.
16. Mogensen, R., Brandell, D., and Younesi, R. (2016). Solubility of the solid electrolyte interphase (SEI) in sodium ion batteries. ACS Energy Lett. *1*, 1173–1178.
17. Nguyen, L.H.B., Camacho, P.S., Fondard, J., Carlier, D., Croguennec, L., Palacin, M.R., Ponrouch, A., Courrèges, C., Dedryvère, R., Trad, K., et al. (2022). First 18650-format Na-ion cells aging investigation: A degradation mechanism study. J. Power Sources *529*, 231253. https://doi.org/10.1016/j.jpowsour.2022.231253.
18. Li, J., Hu, H., Qin, F., Zhang, P., Zou, L., Wang, H., Zhang, K., and Lai, Y. (2017). Flower-like $MoSe_2$/C composite with expanded (0 0 2) planes of few-layer $MoSe_2$ as the anode for high-performance sodium-ion batteries. Chemistry *23*, 14004–14010. https://doi.org/10.1002/chem.201702791.
19. Wang, Q.H., Kalantar-Zadeh, K., Kis, A., Coleman, J.N., and Strano, M.S. (2012). Electronics and optoelectronics of two-dimensional transition metal dichalcogenides. Nat. Nanotechnol. *7*, 699–712. https://doi.org/10.1038/nnano.2012.193.
20. Lei, Z., Zhan, J., Tang, L., Zhang, Y., and Wang, Y. (2018). Recent development of metallic (1T) phase of molybdenum disulfide for energy conversion and storage. Adv. Energy Mater. *8*, 1703482. https://doi.org/10.1002/aenm.201703482.
21. Yang, E., Ji, H., and Jung, Y. (2015). Two-dimensional transition metal dichalcogenide monolayers as promising sodium ion battery anodes. J. Phys. Chem. C *119*, 26374–26380. https://doi.org/10.1021/acs.jpcc.5b09935.
22. Mortazavi, M., Wang, C., Deng, J., Shenoy, V.B., and Medhekar, N.V. (2014). Ab initio characterization of layered MoS_2 as anode for

sodium-ion batteries. J. Power Sources *268*, 279–286. https://doi.org/10.1016/j.jpowsour.2014.06.049.

23. Gao, P., Wang, L., Zhang, Y., Huang, Y., and Liu, K. (2015). Atomic-scale probing of the dynamics of sodium transport and intercalation-induced phase transformations in MoS_2. ACS Nano *9*, 11296–11301. https://doi.org/10.1021/acsnano.5b04950.
24. Wang, X., Shen, X., Wang, Z., Yu, R., and Chen, L. (2014). Atomic-scale clarification of structural transition of MoS_2 upon sodium intercalation. ACS Nano *8*, 11394–11400. https://doi.org/10.1021/nn505501v.
25. Li, Q., Yao, Z., Wu, J., Mitra, S., Hao, S., Sahu, T.S., Li, Y., Wolverton, C., and Dravid, V.P. (2017). Intermediate phases in sodium intercalation into MoS_2 nanosheets and their implications for sodium-ion batteries. Nano Energy *38*, 342–349.
26. Yao, K., Xu, Z., Li, Z., Liu, X., Shen, X., Cao, L., and Huang, J. (2018). Synthesis of grain-like MoS_2 for high-performance sodium-ion batteries. ChemSusChem *11*, 2130–2137.
27. Wang, K., Hua, W., Li, Z., Wang, Q., Kübel, C., and Mu, X. (2021). New insight into desodiation/sodiation mechanism of MoS_2: Sodium insertion in amorphous Mo-S clusters. ACS Appl. Mater. Interfaces *13*, 40481–40488. https://doi.org/10.1021/acsami.1c07743.
28. Yang, B., Wang, Z., Yin, X., Liu, B., Tong, X., Lu, Z., Xie, J., Hu, J., and Cao, Y. (2024). Nano-bowl-like carbon confined 1T/2H-MoS_2 hybrids as anode for high-performance sodium-ion storage. J. Power Sources *597*, 234136. https://doi.org/10.1016/j.jpowsour.2024.234136.
29. Mounet, N., Gibertini, M., Schwaller, P., Campi, D., Merkys, A., Marrazzo, A., Sohier, T., Castelli, I.E., Cepellotti, A., Pizzi, G., and Marzari, N. (2018). Two-dimensional materials from high-throughput computational exfoliation of experimentally known compounds. Nat. Nanotechnol. *13*, 246–252. https://doi.org/10.1038/s41565-017-0035-5.
30. Silva, A., Cao, J., Polcar, T., and Kramer, D. (2022). Design guidelines for two-dimensional transition metal dichalcogenide alloys. Chem. Mater. *34*, 10279–10290. https://doi.org/10.1021/acs.chemmater.2c01390.
31. Silva, A., Cao, J., Polcar, T., and Kramer, D. (2022). Pettifor maps of complex ternary two-dimensional transition metal sulfides. npj Comput. Mater. *8*, 178. https://doi.org/10.1038/s41524-022-00868-7.
32. Wilson, J.A., and Yoffe, A.D. (1969). The transition metal dichalcogenides discussion and interpretation of the observed optical, electrical and structural properties. Adv. Phys. *18*, 193–335. https://doi.org/10.1080/00018736900101307.
33. Chhowalla, M., Shin, H.S., Eda, G., Li, L.J., Loh, K.P., and Zhang, H. (2013). The chemistry of two-dimensional layered transition metal dichalcogenide nanosheets. Nat. Chem. *5*, 263–275.
34. Kuc, A., Zibouche, N., and Heine, T. (2011). Influence of quantum confinement on the electronic structure of the transition metal sulfide TS_2. Phys. Rev. B *83*, 245213. https://doi.org/10.1103/PhysRevB.83.245213.
35. Fan, S., Zou, X., Du, H., Gan, L., Xu, C., Lv, W., He, Y.B., Yang, Q.H., Kang, F., and Li, J. (2017). Theoretical investigation of the intercalation chemistry of lithium/sodium ions in transition metal dichalcogenides. J. Phys. Chem. C *121*, 13599–13605. https://doi.org/10.1021/acs.jpcc.7b05303.
36. Lin, C.H., Topsakal, M., Sun, K., Bai, J., Zhao, C., Dooryhee, E., Northrup, P., Gan, H., Lu, D., Stavitski, E., and Chen-Wiegart, Y.c.K. (2020). Operando structural and chemical evolutions of TiS_2 in Na-ion batteries. J. Mater. Chem. A *8*, 12339–12350. https://doi.org/10.1039/D0TA00226G.
37. Alvarez Ferrero, G., Åvall, G., Mazzio, K.A., Son, Y., Janßen, K., Risse, S., and Adelhelm, P. (2022). Co-intercalation batteries (COIBs): Role of TiS_2 as electrode for storing solvated Na ions. Adv. Energy Mater. *12*, 2202377. https://doi.org/10.1002/aenm.202202377.
38. Ryu, H.S., Kim, J.S., Park, J.S., Park, J.W., Kim, K.W., Ahn, J.H., Nam, T.H., Wang, G., and Ahn, H.J. (2012). Electrochemical properties and discharge mechanism of Na/TiS_2 cells with liquid electrolyte at room temperature. J. Electrochem. Soc. *160*, A338–A343. https://doi.org/10.1149/2.084302jes.
39. Rouxel, J. (1979). Alkali metal intercalation compounds of transition metal chalcogenides: TX_2, TX_3 and TX_4 chalcogenides. In Intercalated Layered Materials (Springer), pp. 201–250.
40. Burns, R.G. (1993). Mineralogical Applications of Crystal Field Theory. In Cambridge Topics in Mineral Physics and Chemistry, Second Edition (Cambridge University Press).
41. Huheey, J., Keiter, E., Keiter, R., and Medhi, O. (2006). Inorganic Chemistry: Principles of Structure and Reactivity, Fourth Edition (Pearson Education).
42. Zuckerman, J.J. (1965). Crystal field splitting diagrams. J. Chem. Educ. *42*, 315.
43. Krishnamurthy, R., and Schaap, W.B. (1969). Computing ligand field potentials and relative energies of d orbitals. J. Chem. Educ. *46*, 799.
44. Phalswal, P., Khanna, P.K., Rubahn, H.G., and Mishra, Y.K. (2022). Nanostructured molybdenum dichalcogenides: a review. Mater. Adv. *3*, 5672–5697.
45. Shuku, Y., Suizu, R., Tsuchiizu, M., and Awaga, K. (2023). Ideal trigonal prismatic coordination geometry of Co(II) in a honeycomb MOF with a triptycene-based ligand. Chem. Commun. *59*, 10105–10108. https://doi.org/10.1039/d3cc02986g.
46. Jahn, H.A., and Teller, E. (1937). Stability of polyatomic molecules in degenerate electronic states I-orbital degeneracy. Proc. R. Soc. Lond. *161*, 220–235.
47. Jahn, H.A. (1938). Stability of polyatomic molecules in degenerate electronic states II-spin degeneracy. Proc. R. Soc. Lond *164*, 117–131.
48. Bartel, C.J. (2022). Review of computational approaches to predict the thermodynamic stability of inorganic solids. J. Mater. Sci. *57*, 10475–10498. https://doi.org/10.1007/s10853-022-06915-4.
49. Genreith-Schriever, A.R., Banerjee, H., Menon, A.S., Bassey, E.N., Piper, L.F.J., Grey, C.P., and Morris, A.J. (2023). Oxygen hole formation controls stability in $LiNiO_2$ cathodes. Joule *7*, 1623–1640. https://doi.org/10.1016/j.joule.2023.06.017.
50. Shadike, Z., Zhou, Y.N., Chen, L.L., Wu, Q., Yue, J.L., Zhang, N., Yang, X.Q., Gu, L., Liu, X.S., Shi, S.Q., and Fu, Z.W. (2017). Antisite occupation induced single anionic redox chemistry and structural stabilization of layered sodium chromium sulfide. Nat. Commun. *8*, 566. https://doi.org/10.1038/s41467-017-00677-3.
51. Xu, Y., Wang, K., Yao, Z., Kang, J., Lam, D., Yang, D., Ai, W., Wolverton, C., Hersam, M.C., Huang, Y., et al. (2021). In situ, atomic-resolution observation of lithiation and sodiation of WS_2 nanoflakes: Implications for lithium-ion and sodium-ion batteries. Small *17*, 2100637. https://doi.org/10.1002/smll.202100637.
52. Morales, J., Santos, J., and Tirado, J.L. (1996). Electrochemical studies of lithium and sodium intercalation in $MoSe_2$. Solid State Ionics *83*, 57–64.
53. Plewa, A., Kulka, A., Hanc, E., Sun, J., Nowak, M., Redel, K., Lu, L., and Molenda, J. (2021). Abnormal phenomena of multi-way sodium storage in selenide electrode. Adv. Funct. Mater. *31*, 2102406. https://doi.org/10.1002/adfm.202102406.
54. Liu, L., Li, B., Wang, J., Du, H., Du, Z., and Ai, W. (2024). Molecular intercalation enables phase transition of $MoSe_2$ for durable Na-ion storage. Small *20*, e2309647. https://doi.org/10.1002/smll.202309647.
55. He, H., Zhang, H., Huang, D., Kuang, W., Li, X., Hao, J., Guo, Z., and Zhang, C. (2022). Harnessing plasma-assisted doping engineering to stabilize metallic phase $MoSe_2$ for fast and durable sodium-ion storage. Adv. Mater. *34*, 2200397. https://doi.org/10.1002/adma.202200397.
56. Yu, Y., Nam, G.H., He, Q., Wu, X.J., Zhang, K., Yang, Z., Chen, J., Ma, Q., Zhao, M., Liu, Z., et al. (2018). High phase-purity 1T'-MoS_2- and 1T'-$MoSe_2$-layered crystals. Nat. Chem. *10*, 638–643. https://doi.org/10.1038/s41557-018-0035-6.
57. Wang, H., Lan, X., Jiang, D., Zhang, Y., Zhong, H., Zhang, Z., and Jiang, Y. (2015). Sodium storage and transport properties in pyrolysis synthesized $MoSe_2$ nanoplates for high performance sodium-ion batteries. J. Power Sources *283*, 187–194. https://doi.org/10.1016/j.jpowsour.2015.02.096.

58. Share, K., Lewis, J., Oakes, L., Carter, R.E., Cohn, A.P., and Pint, C.L. (2015). Tungsten diselenide (WSe_2) as a high capacity, low overpotential conversion electrode for sodium ion batteries. RSC Adv. *5*, 101262–101267. https://doi.org/10.1039/C5RA19717A.

59. Wang, Y., Zhang, X., Xiong, P., Yin, F., Xu, Y., Wan, B., Wang, Q., Wang, G., Ji, P., and Gou, H. (2018). Insight into the intercalation mechanism of WSe_2 onions toward metal ion capacitors: sodium rivals lithium. J. Mater. Chem. A Mater. *6*, 21605–21617.

60. Chaoui, K., Zaari, H., Mansouri, Z., Caballero-Briones, F., Benyoussef, A., El Kenz, A., and Sibari, A. (2025). MoS_2 and WSe_2 monolayers as anode materials for future Li, Na, and K ion batteries under electric field effect. J. Energy Storage *109*, 115110. https://doi.org/10.1016/j.est.2024.115110.

61. Yu, L., He, X., Peng, B., Wang, W., Wan, G., Ma, X., Zeng, S., and Zhang, G. (2023). Constructing ion diffusion highway in strongly coupled WSe2-carbon hybrids enables superior energy storage performance. Matter *6*, 1604–1621. https://doi.org/10.1016/j.matt.2023.03.013.

62. Park, J., Kim, S.J., Lim, K., Cho, J., and Kang, K. (2022). Reconfiguring sodium intercalation process of TiS_2 electrode for sodium-ion batteries by a partial solvent cointercalation. ACS Energy Lett. *7*, 3718–3726.

63. Sun, Y., Åvall, G., Wu, S.H., A Ferrero, G., Freytag, A., Groszewicz, P.B., Wang, H., Mazzio, K.A., Bianchini, M., Baran, V., et al. (2025). Solvent co-intercalation in layered cathode active materials for sodium-ion batteries. Nat. Mater. *24*, 1441–1449. https://doi.org/10.1038/s41563-025-02287-7.

64. Wang, D., Zhao, Y., Lian, R., Yang, D., Zhang, D., Meng, X., Liu, Y., Wei, Y., and Chen, G. (2018). Atomic insight into the structural transformation and anionic/cationic redox reactions of VS_2 nanosheets in sodium-ion batteries. J. Mater. Chem. A *6*, 15985–15992.

65. Pham, D.T., Sambandam, B., Kim, S., Jo, J., Kim, S., Park, S., Mathew, V., Sun, Y.K., Kim, K., and Kim, J. (2018). Dandelion-shaped manganese sulfide in ether-based electrolyte for enhanced performance sodium-ion batteries. Commun. Chem. *1*, 83.

66. Ma, C., Wang, X., Lan, J., Zhang, J., Song, K., Chen, J., Ge, J., and Chen, W. (2023). Dynamic multistage coupling of FeS_2/S enables ultrahigh reversible na–s batteries. Adv. Funct. Mater. *33*, 2211821.

67. Wang, J., Wang, L., Eng, C., and Wang, J. (2017). Elucidating the irreversible mechanism and voltage hysteresis in conversion reaction for high-energy sodium–metal sulfide batteries. Adv. Energy Mater. *7*, 1602706.

68. Ou, X., Xiong, X., Zheng, F., Yang, C., Lin, Z., Hu, R., Jin, C., Chen, Y., and Liu, M. (2016). In situ X-ray diffraction characterization of NbS_2 nanosheets as the anode material for sodium ion batteries. J. Power Sources *325*, 410–416.

69. Agarwal, V., and Chatterjee, K. (2018). Recent advances in the field of transition metal dichalcogenides. Nanoscale *10*, 16365–16397. https://doi.org/10.1039/C7NR07714G.

70. Rasmussen, F.A., and Thygesen, K.S. (2015). Computational 2D materials database: Electronic structure of transition-metal dichalcogenides and oxides. J. Phys. Chem. C *119*, 13169–13183. https://doi.org/10.1021/acs.jpcc.5b02950.

71. Kawamura, M., Narayan, A., Bhutani, A., Rubeck, S., Eckstein, J.N., Shoemaker, D.P., and Wagner, L.K. (2016). Computational and experimental investigation for new transition metal selenides and sulfides: The importance of experimental verification for stability. Phys. Rev. B *94*, 045105. https://doi.org/10.1103/PhysRevB.94.045105.

72. Tedstone, A.A., Lewis, D.J., and O'Brien, P. (2016). Synthesis, properties, and applications of transition metal-doped layered transition metal dichalcogenides. Chem. Mater. *28*, 1965–1974. https://doi.org/10.1021/acs.chemmater.6b00430.

73. Perdew, J.P., Burke, K., and Ernzerhof, M. (1996). Generalized gradient approximation made simple. Phys. Rev. Lett. *77*, 3865–3868. https://doi.org/10.1103/PHYSREVLETT.77.3865.

74. Kresse, G., and Joubert, D. (1999). From ultrasoft pseudopotentials to the projector augmented-wave method. Phys. Rev. B *59*, 1758–1775. https://doi.org/10.1103/PhysRevB.59.1758.

75. Kresse, G., and Hafner, J. (1993). Ab initio molecular dynamics for liquid metals. Phys. Rev. B *47*, 558–561. https://doi.org/10.1103/PhysRevB.47.558.

76. Kresse, G., and Furthmüller, J. (1996). Efficient iterative schemes for ab initio total-energy calculations using a plane-wave basis set. Phys. Rev. B *54*, 11169–11186. https://doi.org/10.1103/PhysRevB.54.11169.

77. Kresse, G., and Furthmüller, J. (1996). Efficiency of ab-initio total energy calculations for metals and semiconductors using a plane-wave basis set. Comput. Mater. Sci. *6*, 15–50. https://doi.org/10.1016/0927-0256(96)00008-0.

78. Grimme, S. (2006). Semiempirical GGA-type density functional constructed with a long-range dispersion correction. J. Comput. Chem. *27*, 1787–1799. https://doi.org/10.1002/jcc.20495.

79. Peelaers, H., and Van de Walle, C.G. (2014). First-principles study of van der Waals interactions in MoS_2 and MoO_3. J. Phys. Condens. Matter *26*, 305502.

80. Ong, S.P., Chevrier, V.L., Hautier, G., Jain, A., Moore, C., Kim, S., Ma, X., and Ceder, G. (2011). Voltage, stability and diffusion barrier differences between sodium-ion and lithium-ion intercalation materials. Energy Environ. Sci. *4*, 3680–3688.